Selective S Cone Damage and Retinal Remodeling Following Intense Ultrashort Pulse Laser Exposures in the Near-Infrared

Christina Schwarz,[*,1] Robin Sharma,[2] Soon Keen Cheong,[†,1] Matthew Keller,[1,3] David R. Williams,[1,4,5] and Jennifer J. Hunter[1,4–6]

[1]Center for Visual Science, University of Rochester, Rochester, New York, United States
[2]Facebook Reality Labs, Redmond, Washington, United States
[3]College of Natural Science, Michigan State University, East Lansing, Michigan, United States
[4]The Institute of Optics, University of Rochester, Rochester, New York, United States
[5]Flaum Eye Institute, University of Rochester, Rochester, New York, United States
[6]Department of Biomedical Engineering, University of Rochester, Rochester, New York, United States

Correspondence: Christina Schwarz, Institute for Ophthalmic Research, University of Tübingen, Elfriede-Aulhorn-Str. 7, Tübingen, 72076, Germany; christina.schwarz@klinikum.uni-tuebingen.de.

Current affiliations: *Institute for Ophthalmic Research, University of Tübingen, Tübingen, Germany. †Department of Ophthalmology, Stanford University, Palo Alto, California, United States.

Submitted: July 30, 2018
Accepted: October 30, 2018

Citation: Schwarz C, Sharma R, Cheong SK, Keller M, Williams DR, Hunter JJ. Selective S cone damage and retinal remodeling following intense ultrashort pulse laser exposures in the near-infrared. *Invest Ophthalmol Vis Sci*. 2018;59:5973–5984. https://doi.org/10.1167/iovs.18-25383

Purpose. Infrared ultrashort pulse lasers are becoming increasingly popular for applications in the living eye. However, safety standards are not yet well established. Here we investigate retinal damage close to threshold for this pulse regime in the living macaque eye.

Methods. Retinal radiant exposures between 214 and 856 J/cm^2 were delivered to the photoreceptor layer with an ultrashort pulse laser (730 nm, 55 fs, 80 MHz) through a two-photon adaptive optics scanning light ophthalmoscope. Retinal exposures were followed up immediately after and over several weeks with high-resolution reflectance and two-photon excited fluorescence ophthalmoscopy, providing structural and functional information.

Results. Retinal radiant exposures of 856 J/cm^2 resulted in permanent S cone damage. Immediately after the exposure, the affected cones emitted about 2.6 times less two-photon excited fluorescence (TPEF) and showed an altered TPEF time course. Several weeks after the initial exposure, S cone outer and inner segments had disappeared. The space was filled by rods in the peripheral retina and cones near the fovea.

Conclusion. Interestingly, S cones are the receptor class with the lowest sensitivity in the near-infrared but are known to be particularly susceptible to ultraviolet and blue light. This effect of selective S cone damage after intense infrared ultrashort pulse laser exposure may be due to nonlinear absorption and distinct from pure thermal and mechanical mechanisms often associated with ultrashort pulse lasers.

Keywords: light damage, ultrashort pulse laser, S cone, visual cycle, two-photon ophthalmoscopy

Femtosecond lasers are nowadays commercially available as turnkey systems and are gaining popularity for retinal applications. These lasers have been used for visual psychophysics in human subjects[1,2] and show promise for ophthalmologic treatment and diagnostic purposes. Femtosecond lasers emit light pulses with much higher peak photon density compared to continuous-wave (CW) lasers at the same average power output. As a result, the likelihood of two-photon events[3,4] is substantially increased[5,6] because of the enhanced probability that a molecule quasi-simultaneously absorbs the energy of two photons. Two-photon absorption at a given wavelength has a similar effect to single-photon absorption at half the wavelength. This feature is of particular interest for retinal applications in the primate eye because the cornea and the crystalline lens absorb wavelengths less than 400 nm and normally prevent these from reaching the retina.[7] Femtosecond lasers in the near-infrared (NIR) take advantage of the optical transmission window at longer wavelengths and can evoke events in the retina that are extremely rare for CW light sources. These highly unnatural illumination conditions raise concern over light safety, especially for the sub-100 fs pulse regime. The consequences of such retinal exposures still lack rigorous investigation, which is also acknowledged in the current *American National Standard for the Safe use of Lasers* (ANSI Z136.1-2014).

At present, ultrashort pulse lasers are used for photodynamic therapy[8,9] and retinal imaging.[10,11] Two-photon excited photodynamic therapy aims to damage tumors[12] or excessive microvessels[9] that develop in wet age-related macular degeneration. The damage is primarily conveyed through drugs that are selectively taken up by the target tissue and become phototoxic upon light exposure. In two-photon excited photodynamic therapy, light damage to the tissue surrounding the target structure must be kept to a minimum. On the other hand, ophthalmoscopy with femtosecond lasers interrogates retinal morphology and physiology through intrinsic fluorophores. Some retinal fluorophores that are relevant for cellular composition,[13] metabolism,[14] and function[15] can only be excited in the ultraviolet (UV) wavelength range and are thus inaccessible in the primate eye[7] with CW lasers. By shifting to

ultrashort pulse lasers, the possibility for two-photon excitation of these fluorophores emerges. Two-photon excited fluorescence (TPEF) ophthalmoscopy in macaque has succeeded in imaging retinal structures[16] that have remained invisible by conventional confocal reflectance imaging. For the first time, retinal ganglion cells could be visualized in the living macaque eye without extrinsic labeling.[16,17] Furthermore, the change in TPEF from photoreceptors over time allows for assessment of visual cycle function. TPEF increases in response to visual stimulation and decreases during dark adaptation.[18] The relative change in fluorescence is well correlated with the amount of visual pigment bleached.[19]

Being a diagnostic technique, TPEF ophthalmoscopy will only succeed if it is truly noninvasive and the required light levels are well below the damage threshold. Previously, we have demonstrated functional TPEF ophthalmoscopy in macaque without indications of retinal damage.[20] Before studies in the human eye are initiated, the first indications of damage that can be observed during TPEF ophthalmoscopy with higher light levels must be explored in an animal model. Here our goal was to establish the damage threshold and investigate damage at threshold in the living macaque with a two-photon adaptive optics scanning light ophthalmoscope for retinal exposures to an ultrashort pulse laser that is suitable for TPEF ophthalmoscopy.

Methods

Animal Preparation

Four *Macaca fascicularis* (three males, aged 5, 10, and 15 years; one female, aged 6 years) with axial length of 17.5 ± 0.8 mm were imaged in this study. Only one eye was imaged per animal. Macaques were handled in accordance with protocols approved by the University of Rochester's Committee on Animal Resources and in compliance with the ARVO Statement for the Use of Animals in Ophthalmic and Vision Research. Imaging sessions lasted for a maximum of 6 hours. A trained animal technician constantly monitored vital signs and recorded these vital signs every 15 minutes. Anesthesia was induced with ketamine (5–20 mg/kg), midazolam (0.25 mg/kg) and glycopyrrolate (0.017 mg/kg) and maintained with isofluorane (1.5%–3%). Paralysis was induced with rocuronium bromide (200–400 mcg/kg/h) and the animal was artificially respirated. The animal was positioned on a stereotaxic cart consisting of an XYZ-stage and a two-axis goniometer, such that the pupil of the eye to be imaged was goniometrically centered. This setup facilitated alignment of the animal's eye with the imaging system and provided access to different retinal locations by moving the animal. The animal's body temperature was maintained at ~38°C with a heated air flow system (Bair hugger; 3M, Maplewood, MN, USA) and warming packs. Lactated Ringer's solution was given via intravenous drip for fluid replenishment. A lid speculum held the eye open, and a contact lens lubricated with eye gel prevented dehydration and corrected for refractive errors. Pupil dilation and cycloplegia were induced with up to 4 drops of phenylephrine hydrochloride (2.5%) and tropicamide (1%). In addition, up to 4 drops of cyclopentolate were given if the pupil did not fully dilate. At the end of the experiment, paralysis was reversed with neostigmine (0.05 mg/kg) and glycopyrrolate (0.01 mg/kg).

Two-Photon Adaptive Optics Scanning Light Ophthalmoscope

Experiments were conducted with a custom two-photon adaptive optics scanning light ophthalmoscope (TP-AOSLO) reported in detail elsewhere.[18] The ultrashort pulse laser (Mai Tai XF-1 with DeepSee attachment, Spectra-Physics, Santa Clara, CA, USA) emitted ~55 fs pulses at 80 MHz and allowed precompensation of second-order dispersion that was induced by the optical system and the eye. The tunable laser was set to emit at 730 nm, and a continuously variable neutral density filter wheel attenuated the beam so that the maximum power for retinal imaging did not exceed 7 mW at the cornea. An 840 nm laser diode (QFLD-850–20S, QPhotonics, Ann Arbor, MI, USA) served for wavefront sensing with a Shack-Hartmann sensor (lenslet array: 203 μm pitch and 7.8 mm focal length; camera; Rolera XR QImaging, Surrey, Canada) and was operated at a maximum power of 45 μW at the cornea. A deformable mirror (DM 97-15, ALPAO SAS, Grenoble, France) corrected the measured aberrations. A superluminescent diode (S-790-G-I-15, Superlum, Carrigtohill, Ireland) with peak emission at 790 nm and maximum power of 200 μW was used for imaging (confocal reflectance mode). Both diodes were cofocused with the pulsed laser at the retina. The focal spot was raster scanned across the retina by a resonant (Electro-Optical Products Corp., Fresh Meadows, NY, USA) and a piezo scanner (S-334.2SL, Physik Instrumente, Karlsruhe, Germany). By changing the curvature of the deformable mirror, the imaging light could be focused at different retinal layers. Two PMT modules (H7422-50, Hamamatsu Photonics, Hamamatsu, Japan) captured light between 780 nm and 800 nm and 710 nm and 750 nm in confocal reflectance configuration. A third PMT (H7422-40, Hamamatsu Photonics, Hamamatsu, Japan) in non-confocal, non-descanned configuration captured TPEF between 400 and 550 nm. The frame rate of the imaging channels was 26.7 Hz. This setup enabled a special paradigm of simultaneous exposure, high-resolution confocal reflectance and TPEF imaging.

Experimental Protocol

Experiments were performed at retinal eccentricities between 2° and 15° from the fovea. Fundus images showing the fovea, optic nerve and blood vessels served as a navigation aid to steer to different retinal locations. The selected areas were imaged in confocal reflectance mode with a field of view of 2.2° × 2° for 20 seconds through the fully dilated pupil to relocate the same location in later imaging sessions. Following 15 minutes of dark adaptation, the photoreceptor layer was exposed to ultrashort pulse laser light over a field of view of 1.3° × 1.1°. During the exposure, reflectance and TPEF videos were captured simultaneously and the TPEF time course was tracked. The imaged location was dark adapted for 15 minutes and followed up immediately after the exposure and again after several weeks. In the immediate follow-up, the PMT gain was maintained and the residual wavefront error was comparable. Tested retinal radiant exposures were 214 J/cm^2, 245 J/cm^2, 428 J/cm^2, 489 J/cm^2, and 856 J/cm^2. Corresponding laser powers and exposure durations are listed in Appendix A, Table A1, and illustrated in Figure 1. For the highest exposure, the same experiment was performed with induced dispersion during the initial exposure, which lead to pulse broadening in the time domain. Dispersion was induced via the dispersion-compensating prism pair inbuilt in the pulsed laser's cavity. Dispersion does not affect the average power but the peak power. The probability of single-photon events is therefore virtually maintained, while the probability of a two-photon event is considerably decreased. Follow-up experiments were always performed with the dispersion-optimized pulsed laser. Images of exposed retinal locations were overlaid on a fundus image so that the characteristic vessel pattern surrounding the area could serve as guidance to re-identify exposed locations at a later time point.

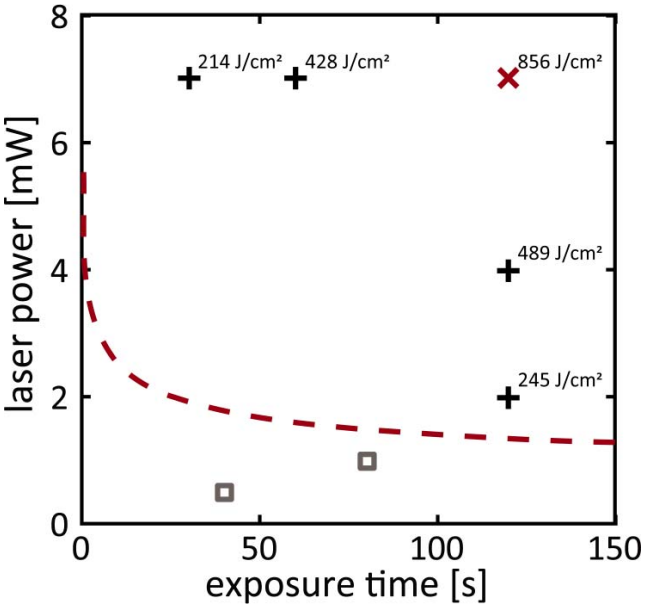

FIGURE 1. Tested exposures in comparison to estimates of maximum permissible exposures (MPEs; *red dashed line*) for the macaque eye. The *red x* marks the exposure where immediate changes were observed. All other exposures did not cause detectable changes (*black crosses*: tested in this study, above MPE; *gray squares*: tested in a previous study,[20] below MPE).

Image Processing and Analysis

During exposure to the ultrashort pulse laser, reflected light and TPEF from the photoreceptors were recorded simultaneously. The reflectance channel delivered a video with high signal-to noise ratio (SNR), whereas the TPEF video had low SNR. Eye motions due to heartbeat and artificially maintained breathing were clearly visible. Cross-correlation–based software computed the displacement between frames and applied a correction to both the high SNR reflectance video and the low SNR TPEF video for dual channel registration.[21] Forward and horizontally flipped backward scans were averaged. Photoreceptors of interest (either all photoreceptors with reduced or maintained TPEF intensity in the follow-up) were marked in registered reflectance images. Binary circular masks with manually selected diameters suitable for the retinal location were applied to TPEF videos in order to extract the TPEF time course. To increase the temporal SNR, TPEF was binned spatially across a group of photoreceptors (i.e., all affected and unaffected photoreceptors during the follow up, respectively).

Histology and Ex Vivo Confocal Microscopy

The oldest monkey was euthanized for histology 1 week after several retinal locations in one eye had been exposed once to 856 J/cm^2. The animal was perfused with 4% paraformaldehyde in 0.1 M phosphate buffer. The eye was enucleated and injected with the fixative. After 1 hour, the eye was dissected, and the retina was separated from the sclera and placed in 4% paraformaldehyde for 2 hours. For wholemount immunostaining, the retina was rinsed with PBS and pretreatment solution (0.4% Triton X-100 in 0.01 M PBS). To reduce nonspecific binding, the retina was incubated in blocking buffer (5% normal horse-serum and 0.4% Triton X-100 in 0.01 M PBS) at room temperature for 4 to 6 hours and then at 4°C overnight. The tissue was incubated in primary antibody solution against S cone opsin (AB5407; EMD Millipore, Billerica, MA, USA) at a dilution of 1:100 at room temperature for 2 hours, then at 4°C for 6 days. After several rinses in PBS, the retina was incubated in secondary antibody goat anti-rabbit coupled to AlexaFluor 568 (ab175471; Abcam, Cambridge, MA, USA) at a dilution of 1:200 at room temperature for 2 hours, then at 4°C for 2 days. Finally, the retina was rinsed, mounted in medium (Vectashield; Vector Laboratories, Burlingame, CA, USA) and coverslipped.

The ex vivo tissue was imaged under a laser scanning confocal microscope (FV1000; Olympus, Tokyo, Japan) with a ×10/0.3 NA microscope objective. DIC mode allowed for steering to the exposed locations as the vessel pattern was clearly visible. Fluorescence from Alexa 568 was captured. Since the flat mounted retina was imaged with the RPE attached, fissures in the RPE were evident. Ex vivo images were high-pass filtered to reduce the visibility of the fissures.

RESULTS

Figure 1 compares the tested exposures to an estimate of the maximum permissible exposure for the macaque eye as proposed in ANSI Z136.1-2014 (see Appendix A). No structural or functional changes were detected for exposures between 214 and 489 J/cm^2 (black crosses; Supplementary Fig. S1). For 856 J/cm^2 (red x), the highest exposure tested, immediate changes were observed as described next.

Laser Exposures Affect Structure and Function of a Subset of Cones

Data that were taken during the initial exposure and the immediate follow-up at a peripheral location are shown in Figure 2. Reflectance (Fig. 2a) and TPEF (Fig. 2c) images captured during the first exposure show regular mosaics of rods and cones in the periphery. The most evident change can be observed in the TPEF follow-up (Fig. 2d). A regularly distributed subset of cones emitted notably less fluorescence than during the first exposure. The same cones were still visible in the reflectance image (Fig. 2b) but appeared smaller in diameter (arrows) or blurred. An animated version of Figure 2 is provided as Supplementary File S2. At the exemplified peripheral retinal location, the affected cones constituted 12% of all cones. During the first exposure (Fig. 2e) TPEF intensity emitted from the unaffected cones increased, peaked and declined. In contrast, TPEF intensity emitted from cones that were identified as affected in the follow-up TPEF images showed a slower initial increase. TPEF intensity from these cones never plateaued but gradually kept increasing for the entire exposure time. At the end of the exposure, similar TPEF intensity to the unaffected cones was reached. During the second exposure (Fig. 2f), both curves of TPEF intensity essentially showed the same trend. However, at the end of the second exposure, the affected cones emitted 2.6 ± 0.2 times less TPEF compared to the end of the first exposure.

A similar analysis was conducted for a near foveal location (~2° from the fovea) where the photoreceptor mosaic consisted of mostly cones (Fig. 3). The brightness of individual cones in reflectance images (Figs. 3a, 3b) varied widely for subsequent exposures. Colocalizing the same cone in consecutive images was often easier based on fluorescence images (Figs. 3c, 3d). An animated version of Figure 3 is provided as Supplementary File S3. About 14% of all cones were affected by the exposure, and the regular distribution (spatial frequency ~13 cyc/deg, Supplementary Fig. S4) was particularly striking. The TPEF time course data (Figs. 3e, 3f) showed the same trend as for the peripheral retinal location.

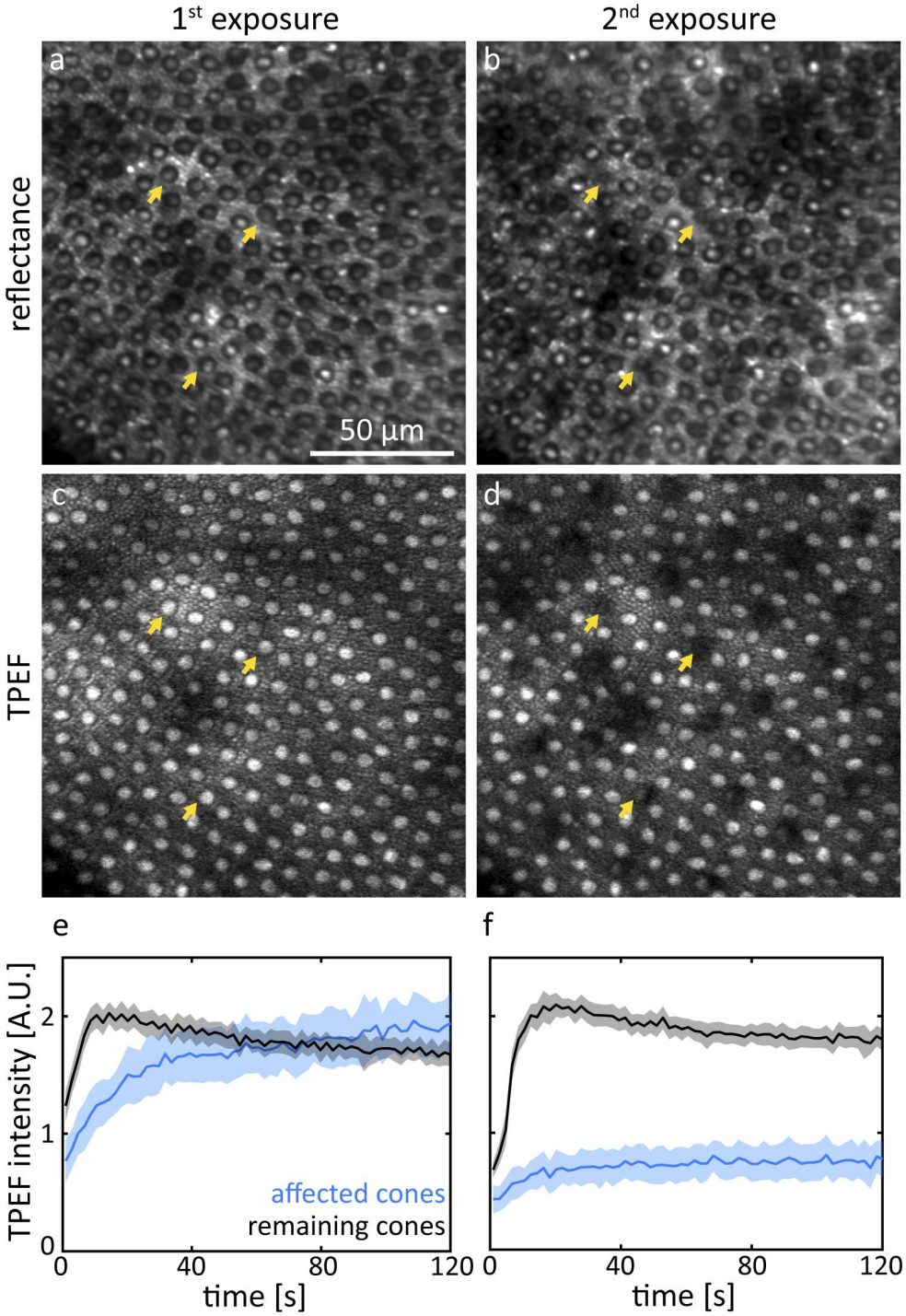

FIGURE 2. Representative reflectance and TPEF images of the same retinal location ~15° from the fovea taken during the first exposure of 856 J/cm^2 (**a**, **c**) and the immediate follow-up (2nd exposure: **b**, **d**). The *yellow arrows* indicate affected cones that appeared decreased in diameter. Cones that emit less TPEF (**e**, **f**) during the 2nd exposure also appear structurally affected in the reflectance image. *Shaded areas* represent SD.

The relative number, the regular distribution, and the distinct response to the imaging laser suggest that the affected cones may be short wavelength sensitive cones (S cones).[22–25]

The Affected Cones Are S Cones

Figure 4 shows TPEF images captured in the living macaque eye during exposure to the ultrashort pulse laser overlaid on a fundus image (Fig. 4a) and histology of the same section of retina stained for S cone opsin (Fig. 4b). At the 856 J/cm^2 exposure sites, which are delimited by solid line corners, S opsin expression was drastically reduced. S cone opsin in outer segments on the far left of the left imaging field might have been protected by the thick vessel that blocked the laser light delivery to the photoreceptor layer. Intrinsic fluorescence from the underlying RPE revealed a largely intact cell mosaic. At the control location exposed to 428 J/cm^2 (delimited by dashed line corners) S cone opsin remained.

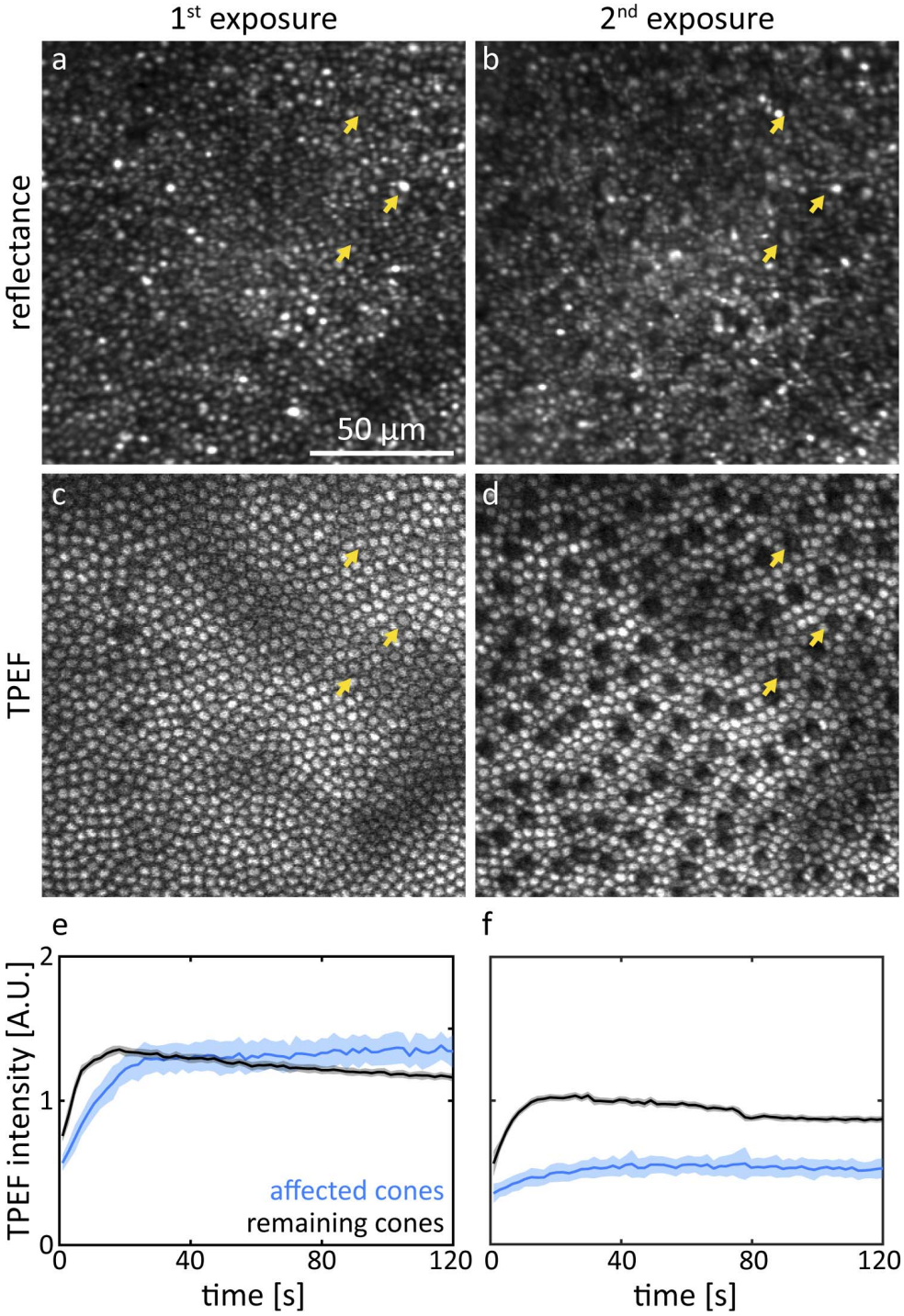

FIGURE 3. Representative reflectance and TPEF images of the same retinal location ~2° from the fovea taken during the first exposure of 856 J/cm^2 (**a**, **c**) and the immediate follow-up (2nd exposure: **b**, **d**). The *yellow arrows* indicate examples of affected cones. The TPEF time course (**e**, **f**) during the 2nd exposure is distinct from that during the 1st exposure. *Shaded areas* represent SD.

The Effect Is Related to the Laser Peak Power

The correlation between the laser peak power and the observed S cone changes was tested by inducing dispersion, which broadened the laser pulses, reducing the laser peak power. Induced dispersion caused an 8-fold decrease in two-photon fluorescence intensity, giving rise to the estimate that the effective pulse duration at the retina was increased likewise by a factor of 8 to ~440 fs. Figure 5 shows TPEF images acquired during the first exposure with the broadened pulse configuration and the immediate follow-up with the usual dispersion-optimized configuration. Even though both images were taken with the same average laser power, the TPEF image acquired with the broadened laser pulses has low SNR and contrast as a result of less efficient two-photon excitation. No changes in structure or function were observed following these pulse-broadened exposures.

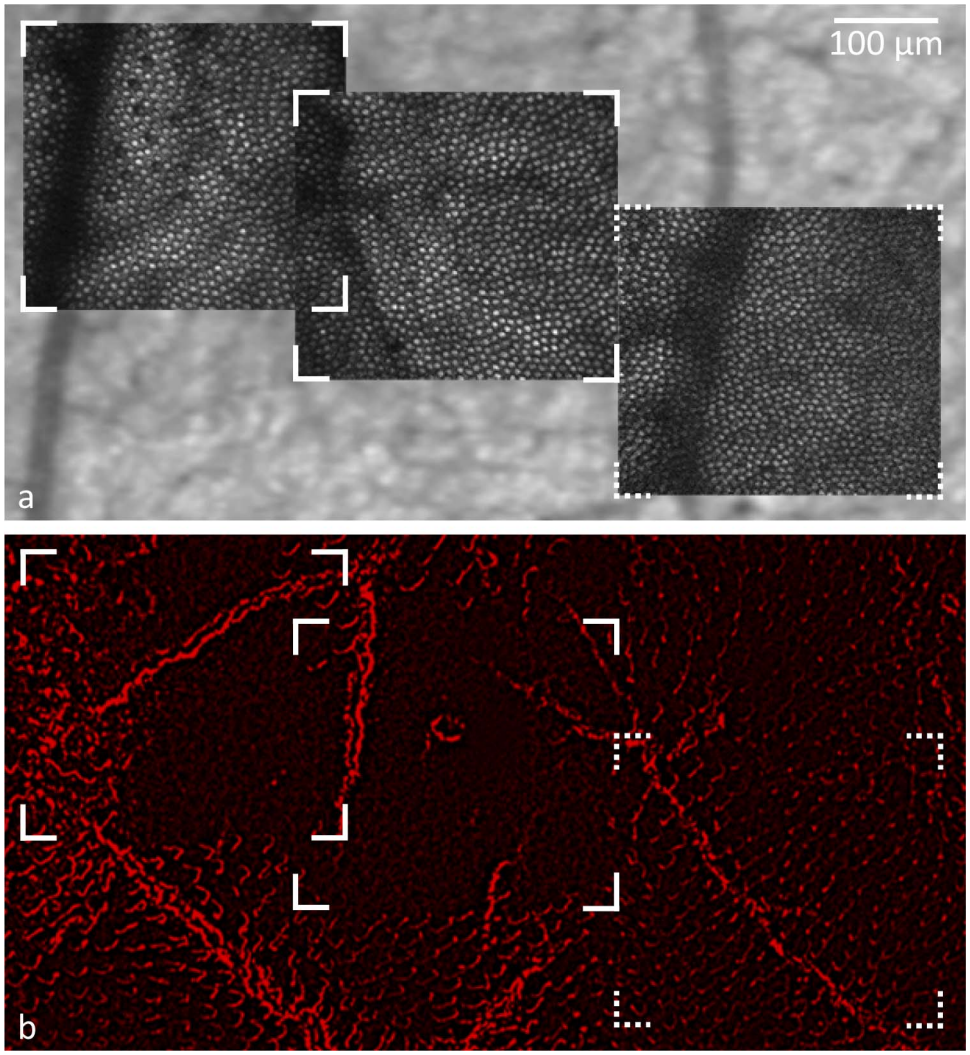

FIGURE 4. S opsin staining was greatly diminished at the 856 J/cm^2 exposure site, but largely remained at the location exposed to 428 J/cm^2. (**a**) In vivo TPEF images of two retinal locations once exposed to 856 J/cm^2 (marked by *solid lines*) and one location exposed to 428 J/cm^2 (marked by *dashed lines*) overlaid on a fundus image. (**b**) Flat-mounted retina of the same location with S opsin stain.

Degeneration of Photoreceptors Leads to Reorganization of the Photoreceptor Mosaic

Remarkably, several weeks after the 856 J/cm^2 exposure had been delivered the targeted locations did not reveal obvious irregularities in the photoreceptor mosaic, even though ~10% of the cones had disappeared. Figure 6 shows reflectance and TPEF images at a peripheral location. By week 3, degenerating cones appeared as dark structures that spread in between neighboring cones. Over the course of weeks, these structures became smaller until they finally disappeared. By week 16, rods had rearranged and filled in the spaces where cones disappeared. Apart from cones that were already affected in week 3 (white arrowheads), several additional cones had disappeared in week 16 (yellow arrows).

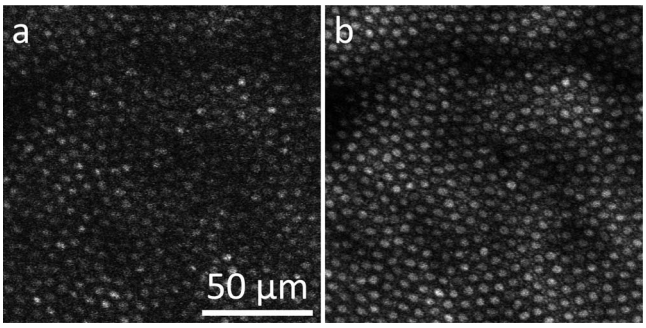

FIGURE 5. No damage was observed following exposures with induced dispersion. Representative TPEF images of the same retinal location taken during the first exposure with broadened pulses (**a**) and the immediate follow-up with optimized pulse duration (**b**).

In another near-peripheral retinal location 1° × 1° in size (Supplementary Fig. S5) that was repeatedly imaged, 18 of 62 cones disappeared. Two observers counted the approximately 1000 surrounding rod outer segments. No change in the number of rods could be detected (change: 37 ± 62 [mean ± SD]), suggesting that these cells redistribute.

Figure 7 shows TPEF images and analysis of near-foveal cone dropout and subsequent redistribution of the surrounding cones. An animated version of this figure is provided as Supplementary Material S6. The foveal photoreceptor mosaic proved to be particularly plastic. Matching up near-foveal pre- and post-exposure images where cones has disappeared was challenging and could only be achieved when a part of the

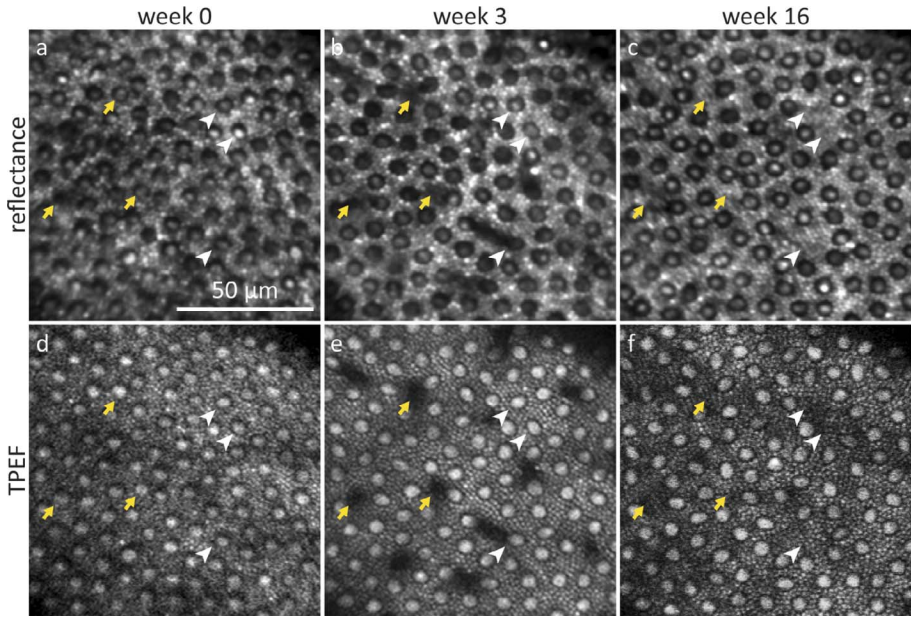

FIGURE 6. Representative reflectance and TPEF images of selective cone degeneration and photoreceptor rearrangement in the near-periphery. Images were taken at the same retinal location during the 856 J/cm^2 exposure (**a**, **d**), in week 3 (**b**, **e**) when cone outer segments were degenerating and in week 16 (**c**, **f**) when the surrounding rods had rearranged. The *yellow arrows* mark cones that were affected by the exposure in week 0, *white arrowheads* mark 3 cones that degenerated after week 3.

imaging field contained intact retina. Cones that surrounded the degenerating cones tended to close the gaps in the photoreceptor mosaic. However, some gaps remained and a number of cones in Figure 7e appeared as if they were not upright but tilted.

DISCUSSION

Manifestation of S Cone Damage

Retinal exposures with ultrashort pulse lasers in the IR can cause selective photoreceptor changes. In vivo imaging and histology suggest that the affected photoreceptors are the short wavelength sensitive cones. S cones differ from M/L cones in many features including topography and morphology.[25] In contrast to human,[26] the central fovea in *Macaca fascicularis* is not S cone free but contains up to 10,000 S cones/mm^2 (Ref. 24). To prevent light damage to the fovea, the most central exposure was delivered at an eccentricity of about 0.5 mm in this study, where 16% of all cones were affected by the imaging light. At a more peripheral location, this percentage dropped to 11%. These numbers agree well with known S cone densities in this species.[24] Furthermore, the affected cones were observed to form a relatively regular submosaic across the retina, which is consistent with S cone topography.[27] Especially in near-foveal locations, some affected cones appeared larger in diameter than the surrounding cones. In ex vivo studies, a greater diameter at the transition of the inner to the outer segment for S cones compared to M/L cones was reported.[26,28] Even though this feature might be detectable here, the increased diameter could also be due to rapid cellular swelling upon stimulation by the imaging laser as has been reported for the photoreceptor outer segment length.[29,30]

In vivo time course images and histology lead us to the conclusion that S cone outer segments atrophy following an 856 J/cm^2 exposure. The injury appears to be specific to S cones, though additional exposures may affect additional cone classes. Changes are visible in reflectance and TPEF images shortly after the exposure. Reflectance images reveal photoreceptor inner and outer segment morphology[31] and wave-guiding properties.[32,33] In registered images taken during the immediate follow up, some affected S cones appeared decreased in diameter or blurred, suggesting that morphologic changes or changes in refractive index had occurred before (or were still occurring while) capturing the video sequence. Changes were also visible in immediate follow-up TPEF images, where the cones appeared darker, but their contour was widely maintained. At the photoreceptor layer the time-varying TPEF signal is mostly due to the fluorophore all-*trans*-retinol.[15]

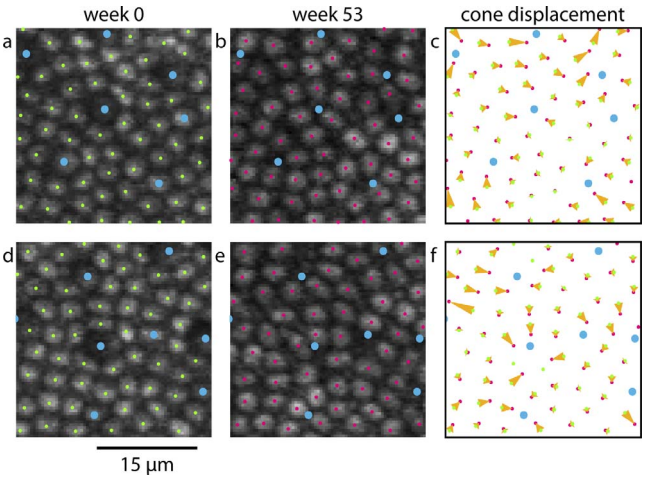

FIGURE 7. As S cones degenerate near the fovea, the remaining cones redistribute. *Blue dots* mark S cones (**a**, **d**) and locations where S cones had degenerated (**b**, **e**). In (**c**) and (**f**), *yellow vectors* illustrate the displacement of cones from their initial position when damage was induced (*green dots*, **a**, **d**) to their position 1 year later (*pink dots*, **b**, **e**).

Reduced fluorescence might imply one of the following situations: First, disruption of the visual cycle may cause a lack of fluorophore. Second, reduced transmittance of excitation light to the fluorophore and/or loss of waveguiding could lead to reduced efficiency of fluorophore excitation. Third, the quantum yield of the fluorophore might decrease due to a change in cellular environment. Fluorescence lifetime ophthalmoscopy (Feeks J, et al. *IOVS* 2017;58:ARVO E-Abstract 3431) may provide further insight as to the reason of TPEF reduction.

The manner in which the appearance of hyporeflective-hypofluorescent patches changed over the course of several weeks is in line with the degeneration of S cones. If the photoreceptor inner segments were maintained, the cone mosaic should show irregularities similar to what has been observed in a patient with acute idiopathic blind spot enlargement.[34] Since we did not observe such irregularities, we infer that at least the outer and inner segments degenerated.

The hyporeflective-hypofluorescent patches that were observed during S cone degeneration may be due to the degenerating part of the photoreceptor becoming opaque and casting a shadow onto the imaging plane with the dark structures that spread in between neighboring cones (Fig. B1) resembling the S cone pedicles. S cone pedicles are smaller than those of other cone classes and make contact with few neighboring cones via gap junctions.[35]

Although S cones (and sometimes additional cones; see white arrowhead in Fig. 6 and Supplementary Fig. S5) degenerate, rods appear to be largely unaffected[36] and fill in the space where cones disappear. Similarly, near the fovea the cones neighboring damaged cones tend to close the gaps in the photoreceptor mosaic; however, some irregularities remain visible. Redistribution of photoreceptors may be guided by least resistance but might involve some active retinal remodeling. Gradual changes in the arrangement and organization of preexisting retinal cells and structures[37,38] have previously been observed following several types of retinal degenerations.

In this study, we did not seek evidence for cell death with immunohistochemistry or TUNEL assay due to the increased difficulty of timing the histology and the risk of damaging the retinal locations of interest. In general, obtaining high quality histology in macaques that are primarily used for in vivo imaging is challenging. First, these animals are extremely valuable for longitudinal imaging experiments and our priority lies in studying the living animal. Consequently, there are not many opportunities to obtain the tissue for ex vivo preparation. Second, the procedure is complicated further because the exposed areas are small and must be located in the flat-mounted tissue. The sections of interest need to be largely free from damage and artifacts. Less artifacts would have been visible, if the RPE had been removed from the retina; however, the delicate outer segments could have been damaged during this procedure. Despite these limitations, the histology shows an apparent reduction of S cone opsin staining consistent with our hypothesis that S cones are affected by intense near-infrared pulsed light exposure. However, more comprehensive histological analysis of the M/L cones, possibly in other animal models or cultured retinae, needs to be undertaken to confirm the selectivity of the reported damage.

Nature of the S Cone Damage Mechanism

Paradoxically, S cones are the receptor class with a spectral sensitivity furthest from the IR illumination that induced the damage,[22,23] but are known to be susceptible to UV and blue light.[39,40] Retinal light damage can occur through several pathways, and a number of theories have been proposed to explain the susceptibility of S cones. The major hypotheses are discussed in light of the present experimental paradigm.

The light levels at which S cone damage was observed exceeded the estimates of thermal maximum permissible exposures by a factor of 5 (see Appendix A). Nevertheless, the appearance of selective photoreceptor injury does not agree with typical thermal damage to the retina, though it is detectable soon after the exposure. Irreversible thermal retinal damage usually occurs following a temperature increase by 10°C. In the eye, melanin absorbs most of the near-infrared light and converts the electromagnetic energy to heat. This pigment is mostly contained within the RPE (and choroid), manifesting as the primary site of thermal damage. Disruption of the RPE cell mosaic has been detected previously by imaging lipofuscin fluorescence.[41] In follow-up images of RPE lipofuscin underlying the exposure sites, we did not detect any irregularities (Supplementary Fig. S7). Even though, choriocapillaries and choroid were not inspected for damage, the possibility that these layers were affected is minor. Given the increased proximity to the focal plane, irregularities in the RPE should be apparent before damage occurs to the vascular layers. The enhanced focusing capabilities adaptive optics provides may explain why the damage was limited to the photoreceptor layer but not the exclusiveness of damage to S cones.

The pulsed emission of the laser could potentially cause mechanical (or acoustic) damage due to compression or tension within the tissue[42] when energy absorption occurs more rapidly than dissipation. Based on calculations that estimate the threshold for mechanical damage,[20] the S cone damaging exposure is too weak for low density plasma formation but generates a free electron density of 2.4×10^{11} cm^{-3}. These free electrons could interact with other substrates via photochemical processes. Photochemical damage is the most common damage and dominates in the UV-visible spectrum especially for long-lasting, low-power exposures. This type of damage is mostly mediated by photosensitizers, such as visual pigments and their bleach products, and requires the presence of oxygen. Upon excitation, the chromophores transfer energy to other substrates, leading to the generation of reactive oxygen species. Photochemical damage to other cell types after comparable exposures to the same kind of laser has been reported previously.[43,44] Photochemical damage selective to photoreceptors is likely to be caused by excessive stimulation.

During femtosecond laser exposures, the photoreceptors are stimulated via single-photon and two-photon pigment isomerization (see Appendix B).[1,2,45] The involvement of a two-photon absorption process in selective S cone damage stands to reason because of the matching action spectrum and the laser peak power playing a role. Exposures delivered in this study stimulated S cones about 4 orders of magnitudes less than L cones. Selective S cone damage can therefore not solely be explained by pigment bleaching. A factor of uncertainty in these calculations is the assumed two-photon absorption cross section (TPXS) of visual pigment, which may differ substantially from the actual curve. Usually the TPXS of a fluorophore tends to be broader and blue shifted with respect to the corresponding single photon action spectrum[46] and for some molecules, such as FAD, the secondary peak in the single photon action spectrum can even result as the most prominent peak for two-photon excitation.[47] Further research is necessary to determine the TPXS of rhodopsin and the cone visual

pigments. Additionally, fluorescence excited at the retina might also contribute to photoreceptor stimulation. Since the detector of the ophthalmoscope is sufficiently sensitive to capture TPEF emitted through the pupil of the eye, it is plausible that a fraction of the TPEF is also absorbed by visual pigment. If 730 nm-excited TPEF in macaque is spectrally comparable to that in mouse (Supplemental Material of Ref. 1), it can cause single-photon pigment isomerizations in all photoreceptors.

The functional response of dark adapted S cones to the onset of the imaging laser in this study suggests that pulsed 730-nm light results in efficient stimulation. Nevertheless, functional responses of S cones to the onset of the imaging light were markedly different from responses of M/L cones. As anticipated, a lower initial rise of TPEF intensity from S cones was observed. However, contrary to expectations, S cones emitted similar amounts of TPEF intensity to M/L cones at the end of the exposure and a clear plateau was not reached. The transient decrease in TPEF intensity during steady illumination was only observed for M/L cones. In a previous study,[18] this behavior has been observed in cones in response to steady-state illumination that instantaneously bleaches all available photopigment. In general, the TPEF time course of S cones was more rod- than M/L cone-like.[18] Despite active investigation, physiologic differences in primate S versus M/L cones are still not fully elucidated due to the sparsity of S cones in the primate retina. However, such physiologic differences could increase the susceptibility of one cone type over the other. In recent studies, immunohistochemistry revealed cone class selective expression of compounds, which spurred speculations on discrepancies in visual cycle and metabolism. It has been proposed that M/L cones might rely on both the traditional[48] and the alternate[49] visual cycle for pigment regeneration,[50] whereas S cones (like rods) have access to only the traditional visual cycle.[51] Our data supports a difference in visual cycle function between S and M/L cones. Further, S cones might use glycolysis as their main energy source, whereas M/L cones use both metabolic pathways (Hoh Kam J, et al. *IOVS* 2017;58:ARVO E-Abstract 3015). Increased presence of oxygen in S cones might also increase the likelihood of photosensitized reactions. Interesting in this regard, is the selective sensitivity loss of the S cone pathway in diseases as diverse as retinitis pigmentosa, diabetes and glaucoma. Common factors in these diseases may be metabolic abnormalities and changes in access to oxygen.[52]

S cone damage has also been proposed to be based on the enhanced rate of pigment regeneration via photoreversal of bleaching,[53] which can occur in the living eye.[54,55] Visual pigment consists of 11-*cis*-retinal covalently bound to an opsin protein. Photon absorption by the visual pigment causes a conformational change of 11-*cis*-retinal to all-*trans*-retinal. Until retinal dissociates the opsin undergoes a series of reactions. The intermediate that persists longest (~s) is metarhodopsin II with an absorption maximum at ~380 nm. Absorption of UV/blue light can re-isomerize the *trans*- to a *cis*-conformation and thus photochemically regenerate visual pigment. In contrast to other studies on blue light damage, our paradigm does not preferentially stimulate S cones but M/L cones. Therefore, if the likelihood for photoreversal of bleaching is the same for all cone types, we have reason to believe that the reported experiments provide evidence against the photoreversal damage theory. While this study does not unravel the mechanism of the selective S cone damage, it emphasizes the benefit of in vivo functional imaging to investigate light damage.

Conclusions

Retinal exposures with IR ultrashort pulsed light can cause selective S cone damage. This unexpected finding is particularly important because the first sign of damage was observed in cells in which single-photon absorption at the illuminating wavelength is extremely low. The effect may be related to a multiphoton event and distinct from pure thermal and mechanical mechanisms often associated with ultrashort pulse exposures. As ultrashort pulse lasers become increasingly popular and commercially available, it might be necessary to revise the current safety guidelines to prevent this type of damage.

Acknowledgments

The authors thank Amber Walker, Lee Anne Schery, Jennifer Strazzeri, and Louis DiVincenti for handling the animals and Tracy Bubel for assistance with histology. Qiang Yang developed the image acquisition and registration software. Adaptive optics control software was developed by Alfredo Dubra and Kamran Ahmad and maintained by Keith Parkins. The cone counting software was developed by Ethan Rossi and Kaccie Li at the University of California, Berkeley. The stereotaxic cart was designed by the United States Air Force Research Laboratories and constructed with modifications by Martin Gira and Mark Dietz at the University of Rochester.

Supported by Research to Prevent Blindness, New York, NY, USA (Unrestricted Grant to the University of Rochester Department of Ophthalmology and a Special Scholars Award to JJH) and National Institutes of Health (P30-EY001319, R01-EY022371, R01-EY004367, R44-AG043645, T32-EY007125, and U01-EY025497). The content is solely the responsibility of the authors and does not necessarily represent the official views of the National Institutes of Health.

Disclosure: **C. Schwarz,** None; **R. Sharma**, Facebook Inc. (E), P; **S.K. Cheong**, None; **M. Keller**, None; **D.R. Williams**, Canon Inc. (F), Canon Inc. (R), P; **J.J. Hunter**, P

References

1. Palczewska G, Vinberg F, Stremplewski P, et al. Human infrared vision is triggered by two-photon chromophore isomerization. *Proc Natl Acad Sci*. 2014;111:5445–5454.
2. Artal P, Manzanera S, Komar K, Gambín-Regadera A, Wojtkowski M. Visual acuity in two-photon infrared vision. *Optica*. 2017;4:1488–1491.
3. Göppert-Mayer M. Über Elementarakte mit zwei Quantensprüngen. *Ann Phys*. 1931;114:273–294.
4. Göppert M. Über die Wahrscheinlichkeit des Zusammenwirkens zweier Lichtquanten in einem Elementarakt. *Naturwissenschaften*. 1929;17:932.
5. Tang S, Tromberg B. Improving the excitation efficiency of multiphoton microscopy using ultrashort pulses. *Adv Imaging*. 2009:NMC3.
6. Tang S, Krasieva TB, Chen Z, Tempea G, Tromberg BJ. Effect of pulse duration on two-photon excited fluorescence and second harmonic generation in nonlinear optical microscopy. *J Biomed Opt*. 2011;11:1–3.
7. Boettner EA, Wolter JR. Transmission of the ocular media. *Invest Ophthalmol Vis Sci*. 1962;1:776–783.
8. Collins HA, Khurana M, Moriyama EH, et al. Blood-vessel closure using photosensitizers engineered for two-photon excitation. *Nat Photonics*. 2008;2:420–424.
9. Khurana M, Moriyama EH, Mariampillai A, Samkoe K, Cramb D, Wilson BC. Drug and light dose responses to focal photodynamic therapy of single blood vessels in vivo. *J Biomed Opt*. 2015;14:1–14.

10. Hunter JJ, Masella B, Dubra A, et al. Images of photoreceptors in living primate eyes using adaptive optics two-photon ophthalmoscopy. *Biomed Opt Express*. 2011;2:139–148.
11. Palczewska G, Dong Z, Golczak M, et al. Noninvasive two-photon microscopy imaging of mouse retina and retinal pigment epithelium through the pupil of the eye. *Nat Med*. 2014;20:785–789.
12. Shen Y, Shuhendler AJ, Ye D, Xu J-J, Chen H-Y. Two-photon excitation nanoparticles for photodynamic therapy. *Chem Soc Rev*. 2016;45:6725–6741.
13. Diaspro A, Chirico G, Collini M. Two-photon fluorescence excitation and related techniques in biological microscopy. *Q Rev Biophys*. 2005;38:97–166.
14. Piston DW, Masters BR, Webb WW. Three-dimensionally resolved NAD(P)H cellular metabolic redox imaging of the in situ cornea with two-photon excitation laser scanning microscopy. *J Microsc*. 1995;178:20–27.
15. Chen C, Tsina E, Cornwall MC, Crouch RK, Vijayaraghavan S, Koutalos Y. Reduction of all-trans retinal to all-trans retinol in the outer segments of frog and mouse rod photoreceptors. *Biophys J*. 2005;88:2278–2287.
16. Sharma R, Williams DR, Palczewska G, Palczewski K, Hunter JJ. Two-photon autofluorescence imaging reveals cellular structures throughout the retina of the living primate eye. *Invest Opthalmology Vis Sci*. 2016;57:632–646.
17. Rossi EA, Granger CE, Sharma R, et al. Imaging individual neurons in the retinal ganglion cell layer of the living eye. *Proc Natl Acad Sci*. 2017;114:586–591.
18. Sharma R, Schwarz C, Williams DR, Palczewska G, Palczewski K, Hunter JJ. In vivo two-photon fluorescence kinetics of primate rods and cones. *Invest Opthalmology Vis Sci*. 2016; 57:647–657.
19. Sharma R, Schwarz C, Hunter JJ, Palczewska G, Palczewski K, Williams DR. Formation and clearance of all- trans -retinol in rods investigated in the living primate eye with two-photon ophthalmoscopy. *Invest Opthalmology Vis Sci*. 2017;58:604–613.
20. Schwarz C, Sharma R, Fischer WS, et al. Safety assessment in macaques of light exposures for functional two-photon ophthalmoscopy in humans. *Biomed Opt Express*. 2016;7:5148–5169.
21. Dubra A, Harvey Z. Registration of 2D images from fast scanning ophthalmic instruments. *Lect Notes Comput Sci*. 2010;6204:60–71.
22. Nunn BJ, Schnapf JL, Baylor DA. Spectral sensitivity of single cones in the retina of Macaca fascicularis. *Nature*. 1984;309: 264–266.
23. Baylor DA, Nunn BJ, Schnapf JL. Spectral sensitivity of cones of the monkey Macaca fascicularis. *J Physiol*. 1987;390:145–160.
24. Bumsted K, Hendrickson A. Distribution and development of short-wavelength cones differ between Macaca monkey and human fovea. *J Comp Neurol*. 1999;403:502–516.
25. Calkins DJ. Seeing with S cones. *Prog Retin Eye Res*. 2001;20: 255–287.
26. Curcio CA, Allen KA, Sloan KR, et al. Distribution and morphology of human cone photoreceptors stained with anti-blue opsin. *J Comp Neurol*. 1991;312:610–624.
27. Shapiro MB, Schein SJ, Monasterio FM de. Regularity and Structure of the Spatial Pattern of Blue Cones of Macaque Retina. *J Am Stat Assoc*. 1985;80:803–812.
28. Ahnelt PK, Kolb H, Pflug R. Identification of a subtype of cone photoreceptor, likely to be blue sensitive, in the human retina. *J Comp Neurol*. 1987;255:18–34.
29. Hillmann D, Spahr H, Pfäffle C, Sudkamp H, Franke G, Hüttmann G. In vivo optical imaging of physiological responses to photostimulation in human photoreceptors. *Proc Natl Acad Sci*. 2016;113:13138–13143.
30. Zhang P, Zawadzki RJ, Goswami M, et al. In vivo optophysiology reveals that G-protein activation triggers osmotic swelling and increased light scattering of rod photoreceptors. *Proc Natl Acad Sci*. 2017;114:2937–2946.
31. Scoles D, Sulai YN, Langlo CS, et al. In vivo imaging of human cone photoreceptor inner segments. *Invest Ophthalmol Vis Sci*. 2014;55:4244–4251.
32. Enoch JM. Nature of the transmission of energy in the retinal receptors. *J Opt Soc Am*. 1961;51:1122–1126.
33. Enoch JM. Waveguide modes: are they present, and what is their possible role in the visual mechanism? *J Opt Soc Am*. 1960;50:1025–1026.
34. Horton JC, Parker AB, Botelho JV, Duncan JL. Spontaneous regeneration of human photoreceptor outer segments. *Sci Rep*. 2015;5:1–10.
35. O'Brien JJ, Chen X, Macleish PR, O'Brien J, Massey SC. Photoreceptor coupling mediated by connexin36 in the primate retina. *J Neurosci*. 2012;32:4675–4687.
36. Palczewska G, Stremplewski P, Suh S, et al. Two-photon imaging of the mammalian retina with ultrafast pulsing laser. *JCI Insight*. 2018;3:1–18.
37. Strettoi E. A Survey of Retinal Remodeling. *Front Cell Neurosci*. 2015;9:1–4.
38. Marc RE, Jones BW, Watt CB, Strettoi E. Neural remodeling in retinal degeneration. *Prog Retin Eye Res*. 2003;22:607–655.
39. Sperling HG, Johnson C, Harwerth RS. Differential spectral photic damage to primate cones. *Vision Res*. 1980;20:1117–1125.
40. Harwerth RS, Sperling HG. Prolonged color blindness induced by intense spectral lights in rhesus monkeys. *Science*. 1971; 174:520–523.
41. Morgan JIW, Hunter JJ, Masella B, et al. Light-induced retinal changes observed with high-resolution autofluorescence imaging of the retinal pigment epithelium. *Invest Ophthalmol Vis Sci*. 2008;49:3715–3729.
42. Youssef PN, Sheibani N, Albert DM. Retinal light toxicity. *Eye (Lond)*. 2011;25:1–14.
43. König K, So PT, Mantulin WW, Tromberg BJ, Gratton E. Two-photon excited lifetime imaging of autofluorescence in cells during UVA and NIR photostress. *J Microsc*. 1996;183:197–204.
44. Tirlapur UK, König K, Peuckert C, Krieg R, Halbhuber K. Femtosecond near-infrared laser pulses elicit generation of reactive oxygen species in mammalian cells leading to apoptosis-like death. *Exp Cell Res*. 2001;263:88–97.
45. Dmitriev VG, Emel'yanov VN, Kashintsev MA, et al. Nonlinear perception of infrared radiation in the 800–1355 nm range with human eye. *Sov J Quantum Electron*. 1979;9:475–479.
46. Xu C, Webb WW. Measurement of two-photon excitation cross sections of molecular fluorophores with data from 690 to 1050 nm. *J Opt Soc Am B*. 1996;13:481–491.
47. Huang S, Heikal AA, Webb WW. Two-photon fluorescence spectroscopy and microscopy of NAD(P)H and flavoprotein. *Biophys J*. 2002;82:2811–2825.
48. Travis GH, Golczak M, Moise AR, Palczewski K. Diseases caused by defects in the visual cycle: retinoids as potential therapeutic agents. *Annu Rev Pharmacol Toxicol*. 2007;47: 469–512.
49. Wang JS, Kefalov VJ. The cone-specific visual cycle. *Prog Retin Eye Res*. 2011;30:115–128.
50. Kiser PD, Zhang J, Sharma A, et al. Retinoid isomerase inhibitors impair but do not block mammalian cone photoreceptor function. *J Gen Physiol*. 2018;150:571–590.
51. Tang PH, Buhushi MC, Ma J-X, Crouch RK. RPE65 is present in human green/red cones and promotes photopigment regen-

Investigative Ophthalmology & Visual Science

eration in an in vitro cone cell model. *J Neurosci*. 2011;31:18618–18626.

52. Greenstein VC, Hood DC, Ritch R, Steinberger D, Carr RE. S (blue) cone pathway vulnerability in retinitis pigmentosa, diabetes and glaucoma. *Invest Ophthalmol Vis Sci*. 1989;30:1732–1737.
53. Cone RA, Brown PK. Spontaneous regeneration of rhodopsin in the isolated rat retina. *Nature*. 1969;221:818–820.
54. Grimm C, Reme CE, Rol PO, Williams TP. Blue light's effects on rhodopsin: photoreversal of bleaching in living rat eyes. *Invest Ophthalmol Vis Sci*. 2000;41:3984–3990.
55. Grimm C, Wenzel A, Williams TP, Rol PO, Hafezi F, Remé CE. Rhodopsin-mediated blue-light damage to the rat retina: Effect of photoreversal of bleaching. *Invest Ophthalmol Vis Sci*. 2001;42:497–505.
56. Delori FC, Webb RH, Sliney DH. Maximum permissible exposures for ocular safety (ANSI 2000), with emphasis on ophthalmic devices. *J Opt Soc Am A Opt Image Sci Vis*. 2007;24:1250–1265.
57. Packer OS, Williams DR. Light, the retinal image and photoreceptors. In: Shevell S, ed. *The Science of Color*. 2nd ed. Boston: Elsevier; 2003:41–102.
58. Baylor DA, Nunn BJ, Schnapf JL. The photocurrent, noise and spectral sensitivity of rods of the monkey macaca fascicularis. *J Physiol*. 1984;357:575–607.
59. Heikkinen H, Nymark S, Koskelainen A. Mouse cone photoresponses obtained with electroretinogram from the isolated retina. *Vision Res*. 2008;48:264–272.
60. Dartnall HJ. The photosensitivities of visual pigments in the presence of hydroxylamine. *Vision Res*. 1968;8:339–358.
61. Hoang QV, Linsenmeier RA, Chung CK, Curcio CA. Photoreceptor inner segments in monkey and human retina: Mitochondrial density, optics, and regional variation. *Vis Neurosci*. 2002;19:395–407.
62. Bowmaker JK, Dartnall HJ, Lythgoe JN, Mollon JD. The visual pigments of rods and cones in the rhesus monkey, Macaca mulatta. *J Physiol*. 1978;274:329–348.
63. Dartnall HJA. The interpretation of spectral sensitivity curves. *Br Med Bull*. 1953;9:24–30.
64. Lamb TD. Photoreceptor spectral sensitivities: Common shape in the long-wavelength region. *Vision Res*. 1995;35:3083–3091.
65. Govardovskii VI, Fyhrquist N, Reuter T, Kuzmin DG, Donner K. In search of the visual pigment template. *Vis Neurosci*. 2000;17:509–528.
66. Denk W, Strickler JH, Webb WW. Two-photon laser scanning fluorescence microscopy. *Science*. 1990;248:73–76.
67. Euler T, Hausselt SE, Breuninger T, et al. Eyecup scope—optical recordings of light stimulus-evoked fluorescence signals in the retina. *Pflugers Arch*. 2009;457:1393–1414.

Appendix A. Laser Safety Calculations

Calculations of MPEs are based on those recommended in the ANSI Z136.1–2014 standard and detailed in previous publications[41,56]; particularly, see Appendix 2 in Schwarz et al.[20] All light sources that emit pulses of pulse durations shorter than 5 µs are considered CW light sources. However, a scanned exposure of the retina by a CW laser can be considered a pulsed exposure.[53]

The imaging wavelength of 730 nm requires calculation of thermal MPEs only (as per ANSI Z136.1–2014). First, the thermal limit of a CW beam uniformly distributed over the entire field is calculated. If exposure durations are within the range $5 \cdot 10^{-6} s \leq t < 3 \cdot 10^{4} s$, the maximum permissible beam power to safely illuminate the retina is given by the following

Table A1. Parameters of the Exposures Tested and MPWs

Retinal Exposure [J/cm^2]	214	428	245	489	856
Exposure duration, s	30	60	120	120	120
Laser power, mW	7	7	2	4	7
MPW, mW	2.0	1.7	1.4	1.4	1.4
Factor above ANSI	1.4	2.8	3.4	4.1	4.9

MPW, maximum permissible laser powers.

equation:

$$MPW_{CW,th} = 1.8 \cdot 10^{-3} \cdot C_A \cdot C_E^* \cdot A_{P,7} \cdot t^{-0.25}$$

with the parameters $C_A = 10^{0.002 \cdot (730-700)} \approx 1.15$ (rough absorption spectrum of melanin), $C_E^* = \frac{22.7\ mrad + 19.2\ mrad}{2 \cdot 1.5\ mrad} \approx 13.96$ (scaling factor for extended, rectangular sources) and $A_{P,7} = \pi \cdot (0.35\ cm)^2 \approx 0.385\ cm^2$ (pupil area 7 mm in diameter).

Next, the thermal limit of a pulsed exposure of a line segment is calculated.[20,41,56] The pulsed line segment (PLS), a rectangular area of length 3.17 mrad and width 1.5 mrad (compare[20]), is exposed during the thermal confinement duration $t_{min} = 5$ µs. During the total exposure, the PLS is scanned more than 40 times (compare[20]), so that the multiple pulse correction factor is $C_P = 0.4$ as determined by ANSI Z 136.1–2014, Table 6C. The maximum permissible beam power is given by

$$MPW_{PLS,th} = 1.8 \cdot 10^{-3} \cdot C_P \cdot C_A \cdot C_{E,PLS}^* \cdot A_{P,7} \cdot t_{min}{}^{-0.25}$$

with the parameters C_A and $A_{P,7}$ being the same as before and the shape factor of the PLS $C_{E,PLS}^* = \frac{3.17\ mrad + 1.5\ mrad}{22.7\ mrad + 19.2\ mrad} \approx 0.11$. For all imaging conditions in this study, the limit for a CW beam uniformly distributed over the entire field is more restrictive than that of a PLS exposures. Here, we apply two additional scaling factors to the limiting maximum permissible beam power MPW_CW,th. The factor $\left(\frac{17}{15}\right)^2$ accounts for the smaller size of the macaque eye compared to the human eye (ratio of focal lengths squared), and the factor $\frac{100}{55}$ accounts for the sub-100 fs pulse duration of the laser (ratio of minimum pulse duration, which the standard is defined for, and pulse duration used here). Maximum permissible laser powers are listed in Table A1.

Appendix B. Photoreceptor Stimulation by the Imaging Laser

The pigment isomerization rates per photoreceptor due to single-photon stimulation by the imaging laser are:

$$n_{1p\_iso} = \phi a_c = \frac{P_{avg} \cdot \lambda \cdot T(\lambda)}{A \cdot h \cdot c} a_c,$$

where ϕ is the photon flux of the stimulating light source of average power, P_{avg}, at the wavelength, λ, illuminating the retinal area, A, through the ocular media with transmittance $T(\lambda)$ at this wavelength,[7,57] h is Planck's constant, and c is the speed of light. The photoreceptor end-on collecting areas[58,59] (neglecting waveguiding) were calculated as follows:

$$a_c = \pi \left(\frac{d}{2}\right)^2 \left[1 - 10^{-\Delta D(\lambda) l}\right] \gamma,$$

where d and l are the average diameter and length of the photoreceptor outer segment (rods: $d_R = 2$ µm, $l_R = 25$ µm; cones: $d_C = 2.1$ µm, $l_R = 13$ µm) and $\gamma = \frac{2}{3}$ is the isomerization efficiency.[60] Rod and cone outer segments are assumed to be cylinders. This assumption is valid for rods and foveal cones.[61] The axial pigment density at the imaging wavelength $\Delta D(\lambda)$ is the product of the photoreceptor's sensitivity

$S(\lambda, \lambda_{max})$ and the axial specific density (rods: 0.019 μm^{-1}; cones: 0.015 μm^{-1}).[62] Relative spectral sensitivities $S(\lambda, \lambda_{max})$ were computed using the standard template[63,64] by Govardovskii et al.[65] λ_{max} of macaque S, M, and L cones were set to 430, 531, and 561 nm[22,23]; λ_{max} of macaque rods was set to 491 nm.[58]

Pigment isomerization rates per photoreceptor due to two-photon stimulation by the imaging laser[1,66,67] were calculated as:

$$n_{2p\_iso} = \sigma(\lambda) g^{(2)} C V \frac{{P_{avg}}^2}{\tau_p \cdot f_{rep}} \left(\frac{NA^2}{\pi h c \lambda}\right)^2 \gamma,$$

where $NA \approx 0.2$ is the numerical aperture of the macaque eye, $V = \pi\left(\frac{d}{2}\right)^2 l$ the volume of the photoreceptor outer segment, C the pigment concentration ($\sim$3.5 mM) and $\sigma(\lambda)$ the two-photon absorption cross-section (TPXS) of the photoreceptor's visual pigment. τ_p and f_{rep} are the imaging laser's pulse duration and repetition rate, $g^{(2)}$ is a factor related to the pulse shape of the laser (e.g., for a Gaussian pulse $g^{(2)} = 0.66$), and all other parameters are the same as above. To our knowledge, the TPXS of visual pigment has not been measured experimentally. However, the maximum TPXS of rhodopsin was estimated based on combined quantum and molecular mechanical simulations as 2.1 GM[1]. In light of the validity of a standard template for single photon absorption of rhodopsin and cone visual pigments, we make the assumption that TPXSs are also well-described by a standard function with the peak wavelength being the only parameter. As a crude approximation, we assumed that $TPXS(\lambda, \lambda_{max}) = 2.1\ \text{GM} \cdot S(\lambda, \lambda_{max})$, resulting in 0.8 GM for S cone opsin and 0.5 GM for rhodopsin and M/L cone opsin at the imaging wavelength.

Figure B1 shows pigment isomerization rates versus average laser power for the two photoreceptor classes, for which two-photon stimulation is least and most efficient, respectively. The single-photon isomerization rate in L cones is about 10^6 times greater than in S cones. For the light levels used, two photon isomerization in S cones is at least a factor of 10 more likely than single-photon isomerization. Two-photon isomerization rates are similar in S and L cones. Broadening the pulse duration by inducing dispersion reduces the two-photon isomerization rates by approximately 1 order of magnitude.

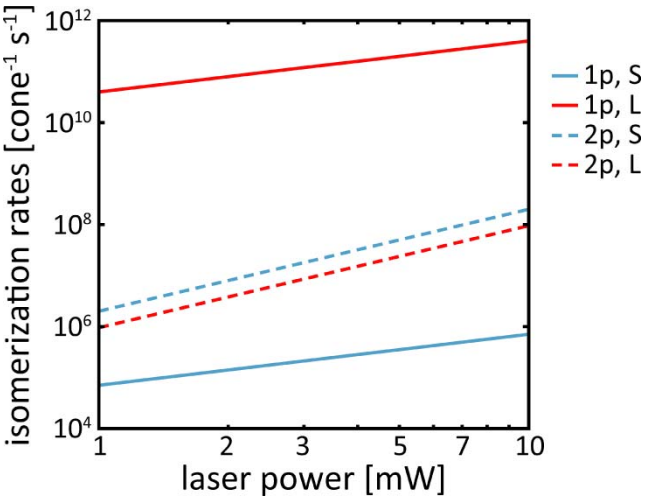

Figure B1. Isomerization rates versus laser power for S and L cones. In S cones, isomerizations after two-photon (2p) absorption are more frequent than after single-photon (1p) absorption, whereas in L cones single-photon isomerizations are most likely.